XL CILAMCE
IBERO-LATIN AMERICAN CONGRESS ON COMPUTATIONAL METHODS IN ENGINEERING
NOVEMBER 11-14, 2019
Praiamar Natal Hotel & Convention Natal, RN-BRAZIL

COLD-FORMED STEEL LIPPED CHANNEL COLUMNS UNDER LOCAL-DISTORTIONAL-GLOBAL BUCKLING MODE INTERACTION

Gustavo Yoshio Matsubara
Eduardo de Miranda Batista
gustavoyoshio@coc.ufrj.br
batista@coc.ufrj.br
COPPE, Civil Engineering Program, Federal University of Rio de Janeiro
Centro de Tecnologia–Bloco I–Sala I216, Ilha do Fundão, CEP 21945-970, Rio de Janeiro/RJ, Brazil.

Abstract. Thin-walled steel cold-formed lipped channel members in axial compression are susceptible to buckling phenomena in the following modes: Local buckling (L), Distortional buckling (D) and Global buckling (G). In these cases, the Direct Strength Method (DSM) predicts the ultimate strength. However, some geometries are affected by the occurrence of coupling phenomena involving two or three buckling modes interaction. The buckling modes interaction produces additional column strength reduction if compared to isolated buckling modes occurrence. Furthermore, the design specifications and codes for cold-formed steel members do not handle properly the ultimate strength for the cases of L-D, D-G and L-D-G interactions. In this context, the present article is aimed at developing a Direct Strength Method (DSM) approach to estimate the ultimate strength of lipped channel columns affected by Local-Distortional-Global buckling mode interaction. To achieve this goal, the investigation is based on: (i) literature review of experimental columns affected by buckling mode interaction (ii) calibration of the FEM model based on experimental results; (iii) nonlinear FEM analysis of post-buckling behavior affected by mode interaction performed with the help of the ANSYS computational program; (iv) propose a Direct Strength Method (DSM) approach to estimate the ultimate strength of lipped channel columns affected by Local-Distortional-Global buckling mode interaction.

Keywords: Steel Cold-Formed Member; Local-Distortional-Global Buckling Mode Interaction; Direct Strength Method (DSM).

1 Introduction

The Brazilian design procedures of steel cold-formed section are described by NBR 14762 [1]. Thus, for practical applications, the use of the Light Steel Frame method is widely used as shown in Fig. 1.

Figure 1 –Light steel frame using cold-formed steel members [2].

The Light steel frame is an efficient and rational way to build. Moreover, there is a time construction decrease and makes the structure lighter. In contrast, these materials present significant instabilities and must be carefully analyzed due to the buckling phenomenon.

There are different buckling modes and each present a different critical load value. The fundamental buckling modes are local buckling (L), distortional buckling (D) and global buckling (G). These fundamental modes are present in Fig. 2.

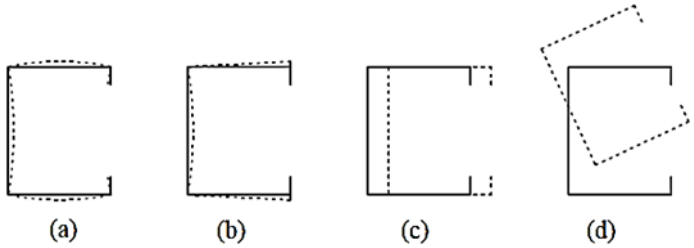

Figure 2 – Buckling modes: (a) local (L), (b) distortional (D), (c) global flexural, (d) global flexural-torsional.

Additionally, these fundamental buckling modes can interact simultaneously with each other. These modes interactions can be local-global buckling (LG), local-distortional buckling (LD), distortional-global buckling (DG) and local-distortional-global buckling (LDG). As a consequence, buckling mode interaction produces additional column strength reduction if compared to isolated buckling mode occurrence.

The LD buckling modes interactions have been more carefully in researches of Dinis *et al.* [4], Silvestre *et al.* [5], Kwon e Hancock [6], Young e Rasmussen [7], Loughlan *et al.*[8], Young *et al.*[9], Martins *et al.* [10], Martins *et al.* [11], Martins *et al.* [12] and Matsubara *et al.* [13].

The DG interaction was researched by Martins *et al.* [14, 15]. Additionally, studies related to LDG interaction were performed by Cava *et al.* [16], Young *et al.* [17], Dinis *et al.* [18], Santos *et al.* [19] and Santos [20].

The most used design methods for buckling modes are Effective Width Method (EWM) (for local buckling mode), Effective Section Method (ESM) (for local and local-buckling buckling mode) and Direct Strength Method (DSM) [22] (for local, distortional and local-global buckling mode). The DSM

[22] originated from a research by Hancock *et al.* [23] and it was included in important standards such as Brazilian standard (NBR 14762[1]), American standard (AISI-S100-16 [24]) and Australian/New Zeland standard (AS/NZS 4600:2005 [25]).

The design procedures for columns subject to local, distortional, global and local-global mode interaction are present in most standards related to the subject. However, studies related to LD, DG and LDG interactions still remain inconclusive.

The present research aims on contributing to propose design approach for LDG buckling mode interaction. The cold-formed lipped channel is one of the most used profiles in steel construction and was chosen for analysis of this article. The cold-formed lipped channel is illustrated in Fig. 3.

Figure 3 – Lipped channel cold-formed steel [3].

2 Design of cold-formed steel columns

The design procedure for cold-formed steel columns experiencing local mode (P_{nL}), distortional mode (P_{nD}) and global mode (P_{nG}) are presented in Eq. (1), Eq. (2), Eq. (3), respectively. The mentioned equations take into account the squash load (P_y=Af_y), local slenderness (λ_L), distortional slenderness (λ_L) and global slenderness (λ_G). The critical local, distortional and global loads are represented by P_{crL}, P_{crD} e $P_{crG,}$ respectively.

$$P_{nL} = \left(1 - \frac{0.15}{\lambda_L^{0.8}}\right)\frac{P_y}{\lambda_L^{0.8}} \quad \text{and} \quad \lambda_L = \sqrt{\frac{P_y}{P_{crL}}} \tag{1}$$

$$P_{nD} = \left(1 - \frac{0.25}{\lambda_L^{1.2}}\right)\frac{P_y}{\lambda_L^{1.2}} \quad \text{and} \quad \lambda_D = \sqrt{\frac{P_y}{P_{crD}}} \tag{2}$$

$$P_{nG} = \begin{cases} \left(0.658^{\lambda_G^2}\right)P_y & for\ \lambda_G \le 1.5 \\ \left(\frac{0.877}{\lambda_G^2}\right)P_y & for\ \lambda_G > 1.5 \end{cases} \quad \text{and } \lambda_G = \sqrt{\frac{P_y}{P_{crG}}} \tag{3}$$

The design of columns subjected to LG interaction is described by Eq. (4) (P_{nLG}). This Equation is created by replacing the squash load (P_y) for P_{nG} (Eq. (3)) in Eq. (1).

$$P_{nLG} = \left(1 - \frac{0.15}{\lambda_{LG}^{0.8}}\right)\frac{P_{nG}}{\lambda_{LG}^{0.8}} \quad \text{and} \quad \lambda_{LG} = \sqrt{\frac{P_{nG}}{P_{crL}}} \tag{4}$$

Schafer [26] propose Eq. (5) for LD interaction of cold-formed columns. It was created similarly to Eq. (4). Thereby, the Equation P_{nDL} was created by replacing the squash load (P_y) for P_{nD} (Eq. (2)) in Eq. (1).

$$P_{nDL} = \left(1 - \frac{0.15}{\lambda_{DL}^{0.8}}\right)\frac{P_{nD}}{\lambda_{DL}^{0.8}} \quad \text{and} \quad \lambda_{DL} = \sqrt{\frac{P_{nD}}{P_{crL}}} \tag{5}$$

Additionally, Schafer [26] propose Eq. (6) for columns experiencing DG buckling mode interaction. This Equation is created by replacing the squash load (P_y) for P_{nG} (Eq. (3)) in Eq. 2.

$$P_{nDG} = \left(1 - \frac{0.25}{\lambda_{DG}^{1.2}}\right)\frac{P_{nG}}{\lambda_{DG}^{1.2}} \quad \text{and} \quad \lambda_{DG} = \sqrt{\frac{P_{nG}}{P_{crD}}} \tag{6}$$

Thereby, for columns experiencing LDG buckling mode interaction, Silvestre *et al.* [27] propose Eq. 7). The main idea of the previously mentioned equations was maintained. Thereby, the squash load was replaced by P_{nDG} (Eq. (6)) in Eq. (1).

$$P_{nDLG} = \left(1 - \frac{0.15}{\lambda_{LDG}^{0.8}}\right)\frac{P_{nDG}}{\lambda_{LDG}^{0.8}} \quad \text{and} \quad \lambda_{LDG} = \sqrt{\frac{P_{nDG}}{P_{crL}}} \tag{7}$$

The design procedures of cold-formed steel, except for global design procedure (Eq. (3)), were based on the equation formulated by Winter [28], represented by Eq. (8). The constants values A and B present in the Winter's Equation are obtained through experimental and/or numerical tests.

$$P_{nW} = \left(1 - \frac{A}{\lambda^B}\right)\frac{P_y}{\lambda^B} \quad \text{and} \quad \lambda = \sqrt{\frac{P_y}{P_{cr}}} \tag{8}$$

3 Column numerical model using the Finite Element Method (FEM)

In order to describe cold-formed steel lipped channel columns behavior, numerical models were developed using ANSYS [29] computational program based on the Finite Element Method (FEM). The SHELL181 element was applied. This element presents a four-node shell element with six degrees of freedom at each node, with translations and rotations about the three-reference axis.

The FEM mesh was taken with 5mm width quadrilateral elements and the material ductility was introduced with bilinear ductile steel elastoplastic development. The details described are present in Fig. 4 and Fig. 5.

The application of the compressive force at both ends was through two concentrated loads in the center of gravity of the profile. Moreover, warping was prevented with 25mm thick plates at both ends. Additionally, the axial displacement in the middle of web was prevented to avoid numerical problems.

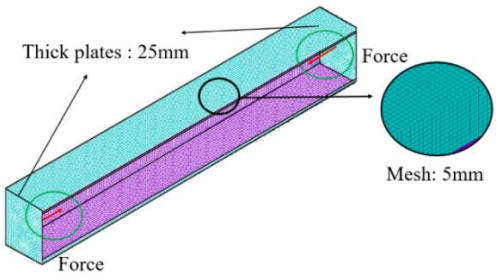

Figure 4 – Shell finite element model of lipped channel CFS column.

A light linear slope (σ/ε) of 1450 MPa was used in the squash load region to avoid convergence problems. The material described is shown in Fig. 5.

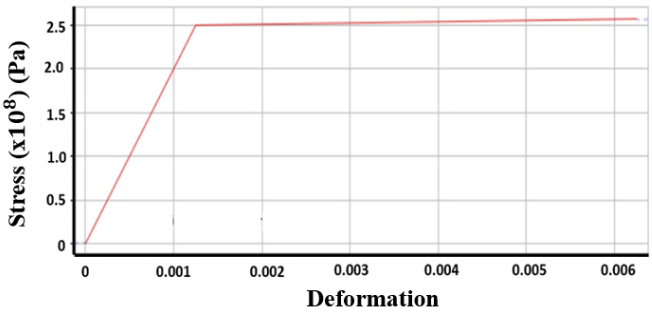

Figure 5 – Bilinear ductile steel elastoplastic.

4 Numerical model performance

The numerical model was evaluated by comparing the ultimate load obtained from numerical tests and the ultimate load obtained from experimental tests. In these cases, the Young modulus and squash load values applied to the numerical columns were obtained through experimental tests by each author.

The experimental tests focused on LD interaction were performed by Kwon and Hancock [6], Young and Rasmussen [7], Loughlan *et al.* [8], Young *et al.* [9], Salles [30]. Additionally, LDG interaction experimental tests were performed by Young *et al.* [17] and Santos [20].

In order to estimate the behavior of experimental tests using numerical models, it was applied the initial imperfections from the previously computed critical buckling mode shape with a maximum amplitude of 10% of the cross-section thickness. Although, some researchers proposed different ways of applying the initial imperfection on numerical models (Pastor *et al.* [31], Schafer and Peköz [32]), the adoption of a maximum imperfection amplitude equal to 10% presents good results, as already verified by Dinis *et al.*[4], Silvestre *et al.* [5], Martins *et al.* [10] and Martins *et al.*[11].

The global initial maximum amplitude equal to L/1000 is adopt form many researchers, e.g. Dinis *et al.* [34]. However, all the experimental columns presented predominant local and/or distortional initial imperfection obtained as the modal shapes from a previously elastic buckling analysis. Therefore, in these cases, the maximum numerical initial amplitude deformation was adopted equal to 10% of the thickness.

The results obtained by means of ANSYS [29] neglect the residual stresses and corner effects - both have been shown to have little impact on the column failure load, as shown in Ellobody and Young [35].

The Riks method [36] was used for nonlinear analysis, as it is the most suitable for dealing with thin-walled instabilities.

The numerical model performance is shown in Fig. 6 obtained with the help of the FEM in comparison with the sets of experimental results provided by Kwon and Hancock [6], Young and Rasmussen [7], Loughlan *et al.* [8], Young *et al.* [9], Salles [30], Young *et al.* [17] and Santos [20]. The results indicate good accuracy regarding the ultimate load ratio P_{uexp}/P_{uFEM}, presenting mean value, standard deviation, and coefficient of variation equal to 0.91, 0.08 and 0.09, respectively.

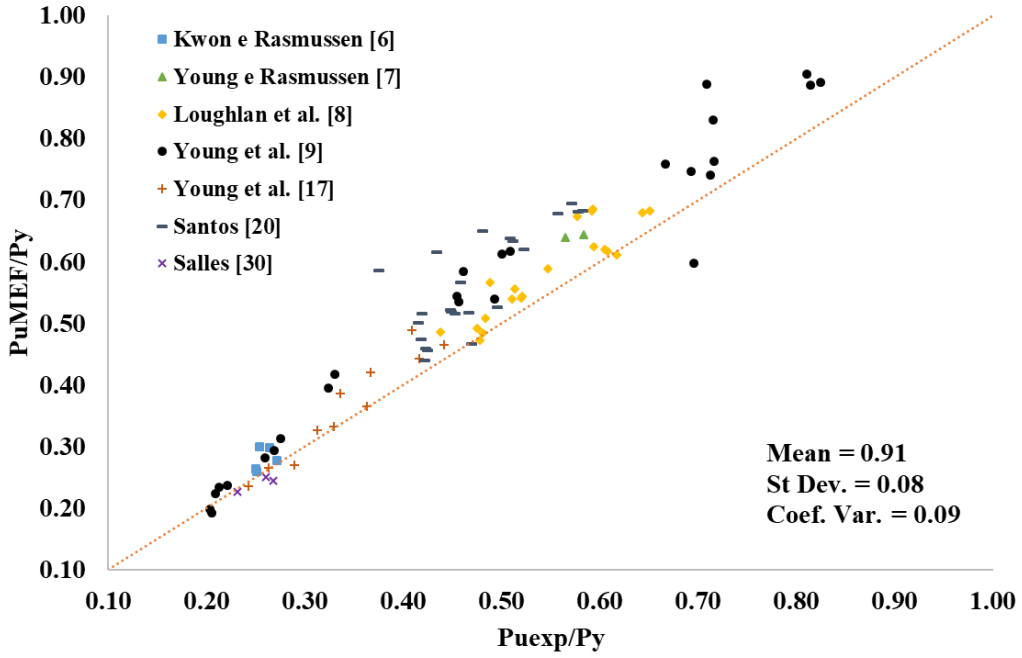

Figure 6 – Comparison between numerical and experimental ultimate loads.

Based on the results in Fig. 6, one should consider the numerical model is adequate to proceed with the computation analysis of lipped channel columns under LD and LDG buckling interaction.

5 Analysis of buckling mode interactions

The research on LDG interaction is based on two steps: (i) propose an approach to deal with LD interaction without the influence of global mode (ii) improve the previous LD approach to deal with the gradual global contribution increase.

5.1 Cold-formed steel under Local-Distortional (LD) buckling interaction

In order to propose an approach to deal with LD interactions, FEM numerical models have been developed to identify the relevant parameters of this phenomenon. To achieve this goal, some considerations were made: (i) the flange-to-web width ratio b_f/b_w is limited between 0.4 and 1.0, the ratio b_s/b_w is limited between 0.1 and 0.3, and the maximum slenderness used was 2.5 (these criteria limit the most common columns used in engineering practice) (ii) the intensity of LD interaction is measured by $R_{\lambda DL} = \lambda_D/\lambda_L$, (iii) the proposed LD approach are based on numerical tests, (iv) the evaluation of the proposed approach will be based on the resistance factor. The element dimension nomenclatures adopted in this article adopted for the lipped channel are shown in Fig. 9.

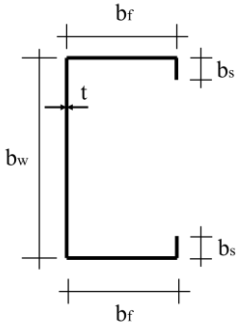

Figure 9 – Nomenclatures adopted for the dimension of a lipped channel, measured from centerline.

The procedure adopted to propose the LD interaction approach was based on 275 numerical tests. At this stage, the global mode of the columns remained very low, presenting ratio λ_G/λ_L and λ_G/λ_D below 0.25. This means that the global critical buckling load was at least 16 times higher than the local and distortional critical buckling loads.

The proposed LD equation was based on the interpolation of the Winter's curve for various values of $R_{\lambda DL}$. Thus, for each interpolated Winter's curve, different values of coefficients A and B were obtained. This methodology was developed by Matsubara *et al.* [13] and it was maintained for this article.

The Fig. 10, Fig. 11 and Fig. 12 illustrate examples of interpolated Winter's curve and for each interpolated curve, four λ_{max} values were used (1.0, 1.5, 2.0 and 2.5).

In Fig. 10, values of A = 0.15 and B = 1.05 are obtained for $R_{\lambda DL}$ = 0.53. The same analysis can be applied to Fig. 11 and Fig. 12.

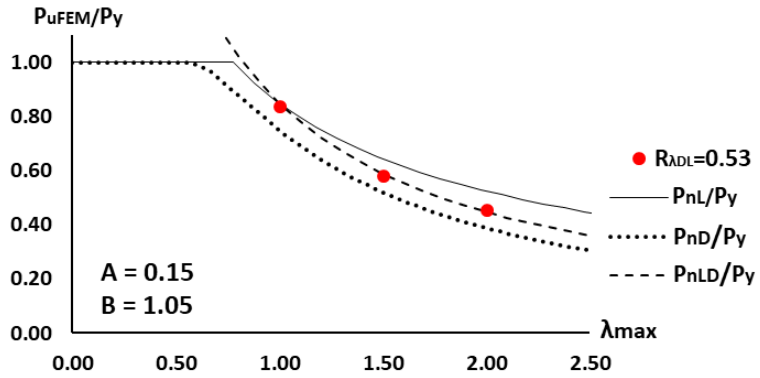

Figure 10 – Winter's curve interpolation (Eq. (8)) for $R_{\lambda DL}$ = 0.53. This interpolation provided constants of A = 0.15 and B = 1.05.

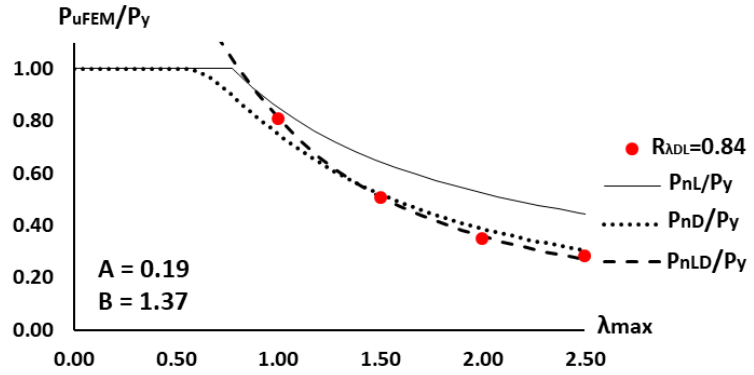

Figure 11 – Winter's curve interpolation (Eq. (8)) for $R_{\lambda DL}$ = 0.84. This interpolation provided constants of A = 0.19 and B = 1.37.

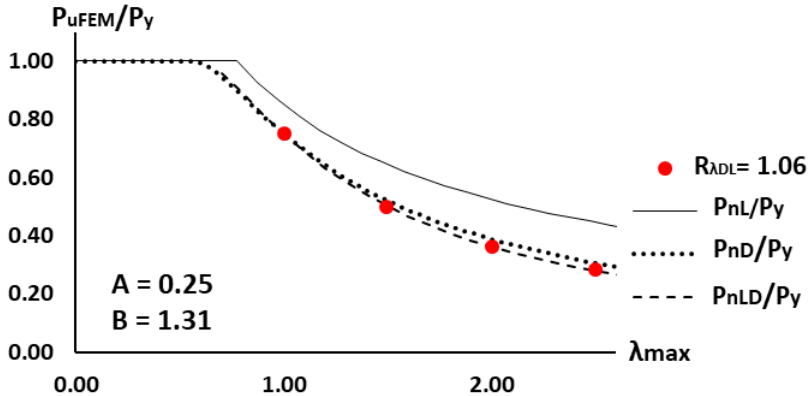

Figure 12 – Winter's curve interpolation (Eq. (8)) for $R_{\lambda DL}$ = 1.06. This interpolation provided constants of A = 0.25 and B = 1.31.

In the numerical tests, 18 different values of $R_{\lambda DL}$ were used, ranging between 0.27 and 1.49. Thus, it was possible to verify the variation of A and B values for different $R_{\lambda DL}$ values, as shown in Fig. 13 and Fig. 14.

The horizontal straight lines on the left side in Fig.13 and Fig.14 represent the constant values of A and B considering the purely local buckling mode. Additionally, the horizontal straight lines on the right side in Fig.13 and Fig.14 represent the constant values of A and B considering the purely distortional buckling mode. It is noticed that between these two lines, the LD interaction behavior is captured.

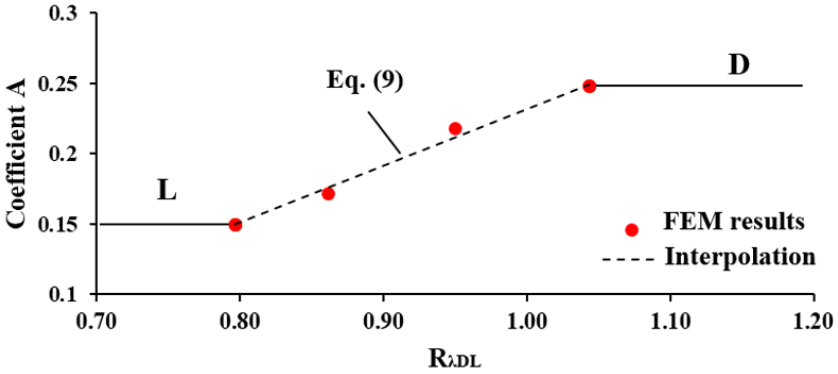

Figure 13 – Variation of the value of A as a function of $R_{\lambda DL}$.

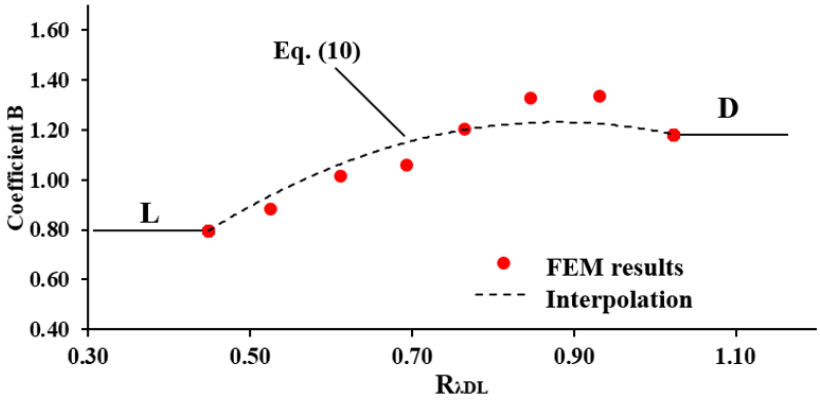

Figure 14 – Variation of the value of B as a function of $R_{\lambda DL}$.

The variations of A and B values for different values of $R_{\lambda DL}$ (Fig. 13 and Fig.14) are described by Eq. (9) and Eq. (10).

$$A = \begin{cases} 0.15 & \text{for} \quad R_{\lambda DL} < 0.80 \\ 0.40\, R_{\lambda DL} - 0.17 & \text{for} \quad 0.80 \leq R_{\lambda DL} \leq 1.05 \\ 0.25 & \text{for} \quad R_{\lambda DL} > 1.05 \end{cases} \tag{9}$$

$$B = \begin{cases} 0.80 & \text{for} \quad R_{\lambda DL} < 0.45 \\ -2.26 {R_{\lambda DL}}^2 + 4.06 R_{\lambda DL} - 0.57 & \text{for} \quad 0.45 \leq R_{\lambda DL} \leq 1.05 \\ 1.20 & \text{for} \quad R_{\lambda DL} > 1.05 \end{cases} \tag{10}$$

The LD interaction is initiated and captured by Eq. (10), starting at $R_{\lambda DL}$ = 0.45 and ending at $R_{\lambda DL}$ = 1.05, this range is the same as found by Matsubara *et al*. [13]. Thereby, P_{nLD} (Eq. (11)) is a proposed approach for columns under local-distortional buckling interaction. The parameter $\lambda_{maxLD} = max\,(\lambda_D, \lambda_L)$ and the values of A and B are obtained by Eq. (9) and Eq. (10).

$$P_{nLD} = \left(1 - \frac{A}{\lambda_{maxLD}^{B}}\right) \frac{P_y}{\lambda_{maxLD}^{B}} \quad \text{for} \quad \begin{matrix} A = \text{Equation 9} \\ B = \text{Equation 10} \end{matrix} \tag{11}$$

The evaluation of the proposed approach, P_{nLD}, for numerical tests in the interaction range ($0.45 \leq R_{\lambda DL} \leq 1.05$) is illustrated in Fig. 15. This graph shows that the ratio between the numerical ultimate load and ultimate load obtained through P_{nLD} (P_{uFEM}/P_{nLD}) presented average, standard deviation and coefficient of variation equal 0.99, 0.10 and 0.10, respectively. These results show that the P_{nLD} Equation is very well adjusted to the numerical tests performed.

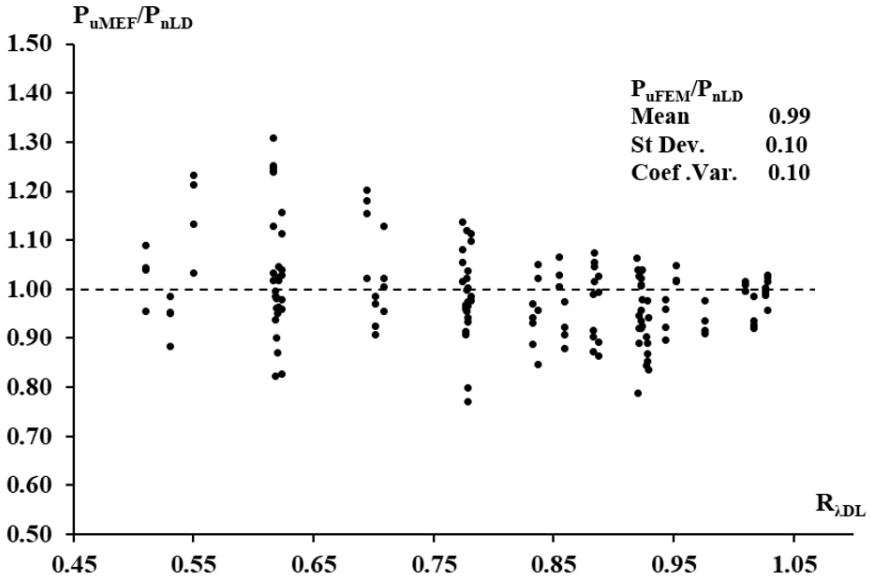

Figure 15 – P_{uFEM} / P_{nLD} ratio variation as a function of $R_{\lambda DL}$. The dashed line represents $P_{uFEM} = P_{nLD}$, considering the interaction range $0.45 \leq R_{\lambda DL} \leq 1.05$.

Additionally, the Fig. 16 illustrates the comparison between experimental tests and P_{nLD} approach. The experimental columns with values well outside the range of $0.4 \leq b_f / b_w \leq 1.0$ and $0.1 \leq b_s / b_w \leq 0.3$ were excluded (due to previously mentioned criteria).

In the Fig. 16, it can be concluded that the P_{nLD} approach is very effective to predict the ultimate experimental load. This conclusion is based on the P_{uexp} / P_{nLD} ratio which presented good results of average, standard deviation and coefficient of variation equal 0.93, 0.11 and 0.12, respectively.

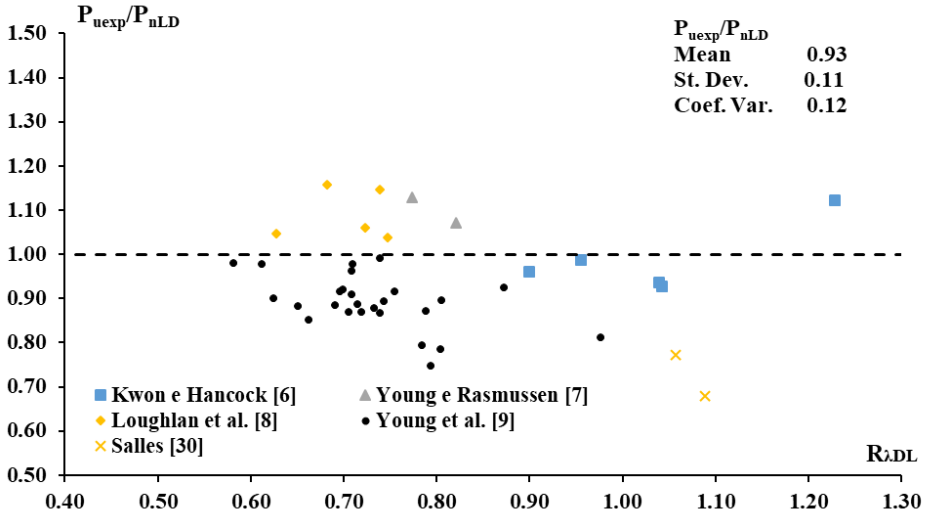

Figure 16 – Ratio between experimental ultimate loads (P_{uexp}) under LD interaction and P_{nLD} approach. The dashed line represents when $P_{uFEM} = P_{nLD}$.

The resistance factor, ϕ, obtained by the P_{nLD} equation presented in good agreement with the values recommended by both the North American standard AISI (2016) and the Brazilian code ABNT (2010),

respectively ϕ= 0.85 and γ= 1.2. The value obtained is ϕ= 0.88 (γ=1/ ϕ=1.14) for numerical tests and 0.85 (γ=1/ ϕ=1.17) for experimental tests. These results can be observed in Table 1.

Table 1 – Values used for the calculation of the resistance factor.

Proposed approach	Equations	Type	γ	ϕ	Number of Columns	Mean	Standard Deviation	Coef. of Variation
P_{nLD}	9,10,11	Exp.	1.17	0.85	40	0.93	0.11	0.12
	9,10,11	Num.	1.14	0.88	160	0.99	0.10	0.10

5.2 Cold-formed steel under Local-Distortional-Global (LDG) buckling interaction

In addition to the analyzes performed so far, we add the experimental tests under LDG interaction performed by Young *et al.* [17] and Santos [20]. Firstly, experimental tests with values well outside of the range $0.4 \leq b_f / b_w \leq 1.0$ and $0.1 \leq b_s / b_w \leq 0.3$ were excluded, as previously done in the study of LD interaction.

Although the P_{nLD} approach was created to handle columns with $\lambda_G / \lambda_{maxLD}$ below 0.25, in Fig. 17 is possible to observe that for the experimental tests analyzed this approach is still effective for values of $\lambda_G/\lambda_{maxLD}$ up to 0.4. When $\lambda_G/\lambda_{maxLD}$ is greater than 0.4, an abrupt drop in resistance occurs due to increased global mode influence.

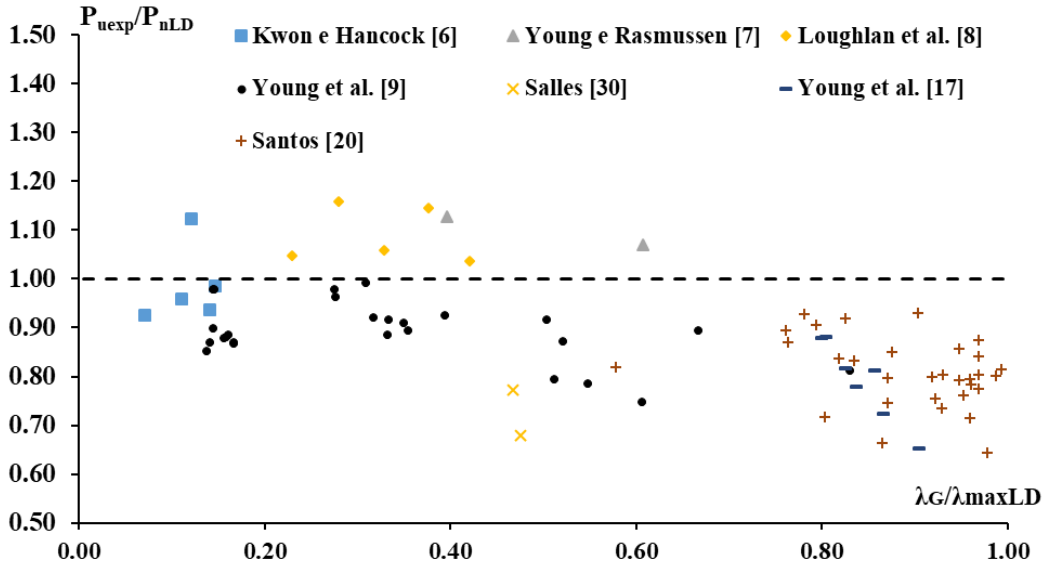

Figure 17 - P_{uexp}/P_{nLD} ratio variation as a function of $\lambda_G/\lambda_{maxLD}$. The dashed line represents when $P_{uexp} = P_{nLD}$.

The experimental columns with high values of $\lambda_G/ \lambda_{maxLD}$ (over 0.7) presented mean, standard deviation and coefficient of variation of P_{uexp}/P_{nLD} ratio equal to 0.80, 0.07 and 0.09, respectively. The low value of mean can be explained by the increased influence of global mode.

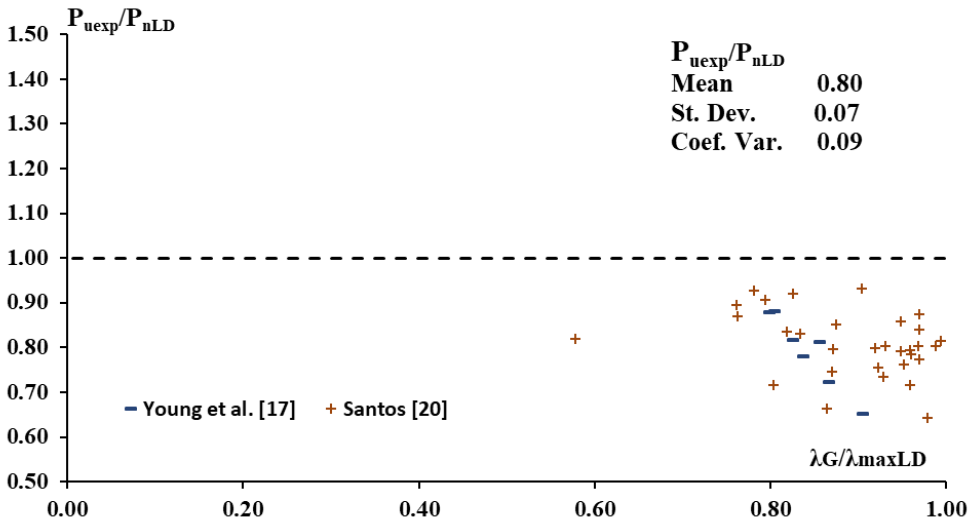

Figure 18 - P_{uexp}/P_{nLD} ratio for different values of $\lambda_G/\lambda_{maxLD}$. The experimental tests were performed by Young *et al.* [17] and Santos [20].

In order to propose an approach that deals with the gradual increase of the global mode, the essence of the methods proposed by Schafer [26] and Silvestre *et al.* [27] were maintained. Thus, to create P_{nLDG} approach, the squash load (P_y) was replaced by P_{nG} (Eq. (3)) in P_{nLD} design approach.

$$P_{nLDG} = \left(1 - \frac{A}{\lambda_{maxLD}^{B}}\right) \frac{P_{nG}}{\lambda_{maxLD}^{B}} \quad \text{for} \quad \begin{matrix} A = \text{Equation 9} \\ B = \text{Equation 10} \\ P_{nG} = \text{Equation 3} \end{matrix} \quad \text{and} \quad \lambda_{LDG} = \sqrt{\frac{P_{nG}}{P_{cr_{minLD}}}} \tag{12}$$

The comparison between experimental ultimate loads under LD interaction γ and the proposed P_{nLDG} equation is shown in Fig. 19. Additionally, the comparison between ultimate load under LDG interaction (Young *et al.* [17], Santos [20]) and the proposed P_{nLDG} approach is presented in Fig. 20.

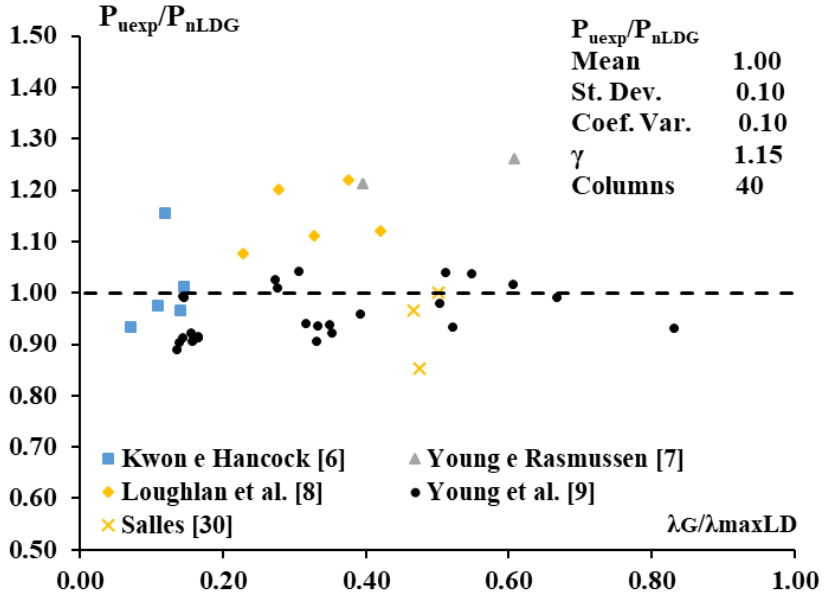

Figure 19 – Comparison between the ratio between experimental ultimate load under LD buckling interaction and P_{nLDG} approach. The distribution of results is a function of the variation of the $\lambda_G/\lambda_{maxLD}$ ratio.

The resistance factor (ϕ) value for experimental columns subjected to LD interaction (Young and Rasmussen [7], Loughlan *et al.* [8], Young *et al.* [9], Salles [30]) using P_{nLDG} approach increased when compared with results obtained by P_{nLD} approach. The increase occurred from 0.85 (γ=1/ϕ=1.17) to 0.87 (γ =1/ϕ=1.15). This increase means an improvement in the results obtained.

In Fig. 20 were considered only experimental columns under LDG interaction (Young *et al.* [17], Santos [20]). In this case, the P_{nLDG} approach obtained good results, presenting resistance factor, ϕ, equal to 0.89 (γ = 1/ϕ=1.12).

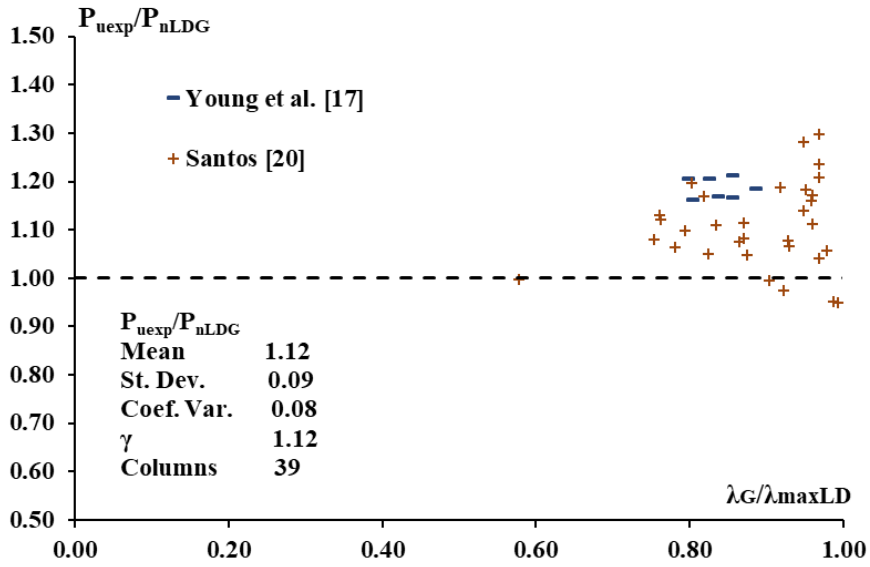

Figure 20 – Evaluation of experimental ultimate load under LDG interaction using P_{nLDG} approach. Note that these columns have high values of $\lambda_G/\lambda_{maxLD}$.

The P_{nLDG} approach presented good results of resistance factor when considering the experimental columns under LD and LDG interaction simultaneously (Table 2). The P_{uexp}/P_{nLDG} ratio values presented mean, standard deviation and coefficient of variation presented values equal to 1.06, 0.11 and 0.11, respectively.

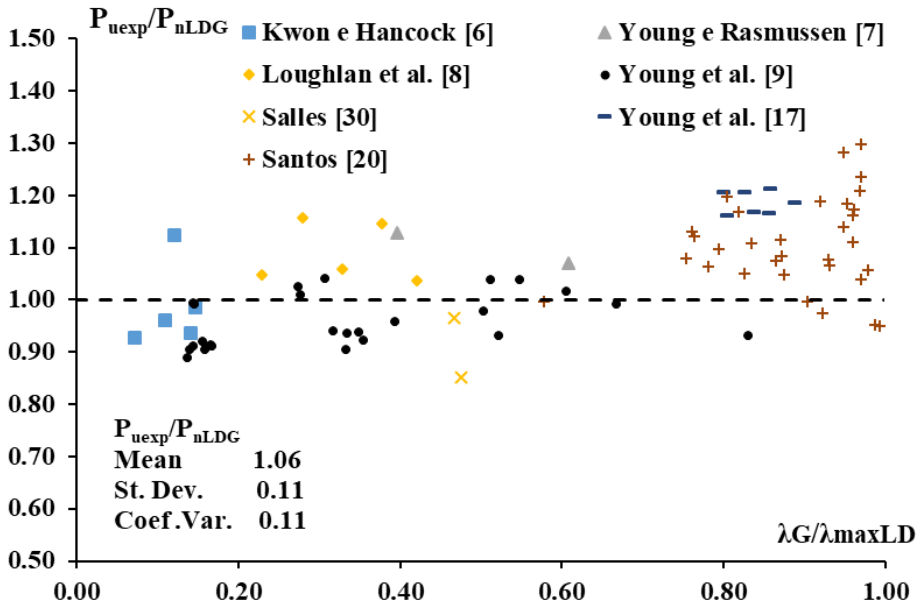

Figure 21 - P_{uexp}/P_{nLDG} ratio variation as a function of $\lambda_G/\lambda_{maxLD}$. The dashed line represents P_{uexp} = P_{nLD}.

Finally, the computation of the resistance factor on the basis of the load and resistance factor design method (LFRD) confirmed adequate performance of the proposed approach, with ϕ= 0.87 (and γ =1/ϕ=1.14) and presented in good agreement with the values recommended by both the North American standard AISI (2016) and the Brazilian code ABNT (2010), respectively ϕ= 0.85 and γ= 1.2. These results can be observed in Table 2.

Table 2 – Values used for the calculation of the resistance factor.

Proposed approach	**Equations**	**Type**	**γ**	**ϕ**	**Number of columns**	**Mean**	**Standard Deviation**	**Coef. of variation**
P_{nLDG}	9,10,12	Exp.	1.14	0.87	79	1.06	0.11	0.11

6 Conclusions

This article aimed to contribute to the development of knowledge about buckling mode interaction. Thus, to achieve this goal, a numerical model in MEF was developed to estimate the ultimate load of cold-formed steel lipped channel. The results obtained in this article is an extension of previous results recently published by the authors in Matsubara et al. [13].

The proposed P_{nLD} approach was based on numerical models in MEF to deal with lipped channel cold-formed steel under LD buckling interaction. The resistance factor obtained for numerical and experimental tests were 0.88 (γ=1/ ϕ=1.14) and 0.85 (γ=1/ϕ=1.17), respectively. These results confirmed adequate performance of the P_{nLD} approach. These values were in good agreement with the values recommended by both the North American standard AISI (2016) and the Brazilian code ABNT (2010), respectively ϕ = 0.85 and γ = 1.20.

Additionally, the proposed P_{nLDG} approach aims to estimate the ultimate load of columns subject to LDG buckling mode and very good results were obtained in these cases. The resistance factor obtained for LDG experimental tests was 0.89 (γ=1/ ϕ=1.12). Furthermore, P_{nLDG} approach was also effective to estimate the ultimate load of steel columns subjected to LD and LDG mode interaction, presenting ϕ = 0.87 (γ=1/ϕ=1.14).

Finally, additional numerical and experimental tests focused on DG buckling interaction and numerical tests focused on LDG are underway to better support the proposed P_{nLDG} approach.

Acknowledgements

The first author acknowledges the financial support of CNPq, National Council for Scientific and Technological Research, through scholarship for his Doctoral degree research.

References

[1] ABNT. NBR 14762: Dimensionamento de Estruturas de Aço constituídas por Perfis Formado a Frio. Brasil, Brazilian Association of Technical Standards, 2010.
[2] GYPSTEEL, 2011. Produtos Steel Frame. Available: < http://www.gypsteel.com.br/>. Access in: 24 de June de 2019.
[3] PERFIL NORTE, 2011. Catálogo Perfil Norte. Available: <http://www.perfilnorte.com >. Access in:18 January. 2019.
[4] P.B. Dinis, D. Camotim, N. Silvestre. FEM-based analysis of the local-plate/distortional mode interaction in cold-formed steel lipped channel columns. *Computers and Structures*, vol. 85, pp. 1461–1474, 2007.
[5] N. Silvestre, D. Camotim, P.B. Dinis. Post-buckling behaviour and direct strength design of lipped channel columns experiencing local/distortional interaction. *Journal of Constructional Steel Research*, vol. 73, pp. 12–30, 2012.
[6] Y.B. Kwon, G.J. Hancock. Tests of cold-formed channels with local and distortional buckling. *Journal of Structural Engineering*, vol. 118: pp. 1786–1803, 1992.
[7] B. Young, K.J.R. Rasmussen. Design of lipped channel columns. *Journal of Structural Engineering*, vol. 124: pp. 140–148, 1998.
[8] J. Loughlan, N. Yidris, K. Jones. The failure of thin-walled lipped channel compression members due to coupled local-distortional interactions and material yielding. *Thin-Walled Structures*, vol. 61, pp. 14–21, 2012.
[9] B. Young, N. Silvestre, D. Camotim. Cold-Formed Steel Lipped Channel Columns Influenced by Local-Distortional Interaction: Strength and DSM Design. *Journal of Structural Engineering*, vol. 139, pp. 1059–1074, 2013.
[10] A.D. Martins, D. Camotim, P.B. Dinis, B. Young. Local-Distortional Interaction in Cold-formed Steel Columns: Mechanics, Testing, Numerical Simulation and Design. Structures, vol. 4: pp. 38–57, 2015a.
[11] A.D. Martins, P.B. Dinis, D. Camotim, P. Providência. On the relevance of local-distortional interaction effects in the behaviour and design of cold-formed steel columns. Computers and Structures, vol. 160, pp. 57–89, 2015b.
[12] A. D. Martins, D. Camotim, P.B. Dinis. On the direct strength design of cold-formed steel columns failing in local-distortional interactive modes. *Thin-Walled Structures*, vol. 120, pp. 432–445, 2017.
[13] G.Y. Matsubara, E.M. Batista, G.C. Salles. Lipped channel cold-formed steel columns under local-distortional buckling mode interaction. *Thin-Walled Structures*, vol. 137: pp. 251–270, 2019.
[14] A.D. Martins, D. Camotim, R. Gonçalves, P.B. Dinis. On the mechanics of distortional-global interaction in fixed-ended columns. *Thin-Walled Structures*, vol. 123, pp. 162-184, 2018.
[15] A.D. Martins, D. Camotim, P.B. Dinis. On the distortional-global interaction in cold-formed steel columns: Relevance, post-buckling behaviours, strength and DSM design. *Journal of Constructional Steel Research*, vol. 145, pp. 449-470, 2018.
[16] D. Cava, D. Camotim, P.B. Dinis, A. Madeo. Numerical investigation and direct strength design of cold-formed steel lipped channel columns experiencing local-distortional-global interaction. *Thin-Walled Structures*, vol. 105, pp. 231-247, 2016.
[17] B. Young, P.B. Dinis, D. Camotim. CFS lipped channel columns affected by L-D-G interaction. Part I: Experimental Investigation. *Computers and Structures*, vol. 207, pp. 219-232, 2017.
[18] P.B. Dinis, D. Camotim, B. Young, E.M. Batista. CFS lipped channel columns affected by L-D-G interaction. Part II: Numerical simulations and design considerations. *Computers and Structures*, vol. 207, pp. 200-218, 2018.
[19] E.S. Santos , E.M. Batista, D. Camotim. CFS lipped channel columns affected by L-D-G interaction. Part II: Numerical simulations and design considerations. *Computers and Structures*, vol. 207, pp. 200-218, 2018.
[20] E.S. Santos. Interação entre os modos de flambagem local-distorcional-global em perfis de aço formados a frio com seção U enrijecido na compressão axial. Tese de Doutorado, COPPE/ Universidade Federal do Rio de Janeiro, 2014.

[21] E.M. Batista. Effective section method: A general direct method for the design of steel cold-formed members under local-global buckling interaction. *Thin-Walled Structures*, vol. 45, pp. 345–356, 2010.
[22] B.W. Schafer, T. Peköz, 1998. Direct strength prediction of cold-formed steel members using numerical elastic buckling solutions, 1998. In: LaBoube R, Yu W-W, (Eds.). Proceedings of 14th international specialty conference on cold-formed steel structures (St. Louis, 15-16-10), pp. 69-76.
[23] G.J. Hancock, Y.B. Kwon, E.S. Bernard. Strength design curves for thin-walled sections undergoing distortional buckling. *Journal Construction*, vol.31, pp. 169-186, 1994.
[24] AISI, 2016. North American Specification for the Design of Cold-Formed Steel Structural Members (AISI-S100-16), American Iron and Steel Institute, Washington DC.
[25] AS/NZS, 2005. *Cold-Formed Steel Structures*, Standards of Australia (SA) and Standards of New Zealand (SNZ), Sydney-Wellington.
[26] B.W. Schafer. Local, distortional and Euler buckling in thin-walled columns. *Journal of Structural Engineering*, vol. 128, pp. 289-299, 2002.
[27] N. Silvestre, P.B. Dinis, D. Camotim, E.M. Batista, 2010. DSM design of lipped channel columns undergoing local/distortional/global mode interaction. In: Proceedings of SDSS'Rio 2010 Stability and Ductility of Steel Structures (Rio de Janeiro, Brasil), vol. 2, pp. 1061-1068.
[28] G. Winter, 1968. Thin-Walled Structures-Theoretical Solutions and Test Results. In: Preliminary Publications of the Eight Congress (IABSE), pp. 101-112.
[29] SAS. Theory Reference for the Mechanical APDL and Mechanical Applications, 2009.
[30] G.C. Salles. Investigação analítica, numérica e experimental do modo de flambagem distorcional em perfis formados a frio. M. Sc dissertation, COPPE/ Federal University of Rio de Janeiro, 2017.
[31] M. M. Pastor, M. Casafont, J. Bonada, F. Roure. Imperfection amplitudes for nonlinear analysis of open thin-walled steel cross-sections used in rack column uprights. *Thin-Walled Structures*, vol. 76, pp. 24-41, 2014.
[32] B.W. Schafer, T. Peköz. Computational modeling of cold-formed steel: characterizing geometric imperfections and residual stresses. *Journal of Constructional Steel Research*, vol. 47, pp. 193-210, 1998.
[33] B.W. Schafer, T. Peköz. Computational modeling of cold-formed steel: characterizing geometric imperfections and residual stresses. *Journal of Constructional Steel Research*, vol. 47, pp. 193-210, 1998.
[34] P.B. Dinis, D. Camotim, A. Landesmann, A.D. Martins. On the direct strength method design of columns against global failures. *Thin-Walled Structures*, vol. 139, pp. 242-270, 2019.
[35] E. Ellobody, B. Young. Behavior of Cold-Formed Steel Plain Angle Columns. *Journal of Structural Engineering*, vol. 131, pp. 457-466, 2005.
[36] E. Riks. An icremental approach to the solution of snapping and buckling problems. *Internacional Journal of solids and structures*, vol. 15, pp. 529-551, 1979.